CONF-890721--31

A Method for Three-Dimensional Structural Analysis of Reinforced Concrete Containment

CONF-890721--31

DE89 013306

R. F. Kulak and C. Fiala

Reactor Analysis and Safety Division
Argonne National Laboratory
Argonne, Illinois 60439

DISCLAIMER

ABSTRACT

A finite element method designed to assist reactor safety analysts in the three-dimensional numerical simulation of reinforced concrete containments to normal and off-normal mechanical loadings is presented. The development of a lined reinforced concrete plate element is described in detail, and the implementation of an emperical transverse shear failure criteria is discussed. The method is applied to the analysis of a 1/6th scale reinforced concrete containment model subjected to static internal pressurization.

INTRODUCTION

The containment structure is the final barrier between fission products released inside the containment during accidents and the atmosphere. Containments have been designed in cylindrical configurations, spherical configurations, and rectilinear configurations. Penetrations such as equipment hatches, personnel locks, etc. disrupt the smoothness of the pressure boundary and can create stress and/or strain concentrations. Reinforced concrete (RC) is used as a building material for nuclear reactor containments throughout the world because of the wide availability of reinforcing bars, cement, and gravel. Compared to other construction methods, it is relatively economical.

In order to determine the performance of these structures to normal and off-normal loadings, it is necessary to perform numerical simulations. Because of the complex three-dimensional geometry of the containment structures and the presence of penetrations, it is necessary to perform three-dimensional analysis. This paper describes a finite element method that may be used to analyze the structural response of RC containment structures to pressure loadings. The method has been coded in the NEPTUNE computer program (Kulak and Fiala, 1988), which is a three-dimensional nonlinear mechanics finite element code.

The second section describes a lined, reinforced concrete plate element that is used to model concrete structural components such as walls, floors, ceilings, etc. A terse formulation of the basic element is first presented; the formulation for arbitrarily positioned reinforcing bars is then developed; and a liner model that accounts for the liner's membrane response is discussed. The third section describes the material models used to represent concrete, reinforcing bars, and liner steel. The failure criteria for each of the above components is discussed as well as an emperical criteria for transverse shear failure. The solution algorithms for static and dynamic loadings are described in the fourth section. The fifth section describes display techniques used to visualize the layered reinforcing bars within the concrete sections and the predicted cracking and crushing patterns during loading. The application of the method to pretest simulations of the response of a RC containment model is described in the sixth section.

LINED REINFORCED CONCRETE PLATE ELEMENT

Most containment structures can be modelled with plate elements. Thick RC sections, such as the base mat, would have to be modelled with continuum elements, which are not here considered.

Quadrilateral Plate Element

Our evaluation of the available formulations indicated that the bilinear four-node quadrilateral plate element (Fig. 1) formulation proposed by Belytschko et al. (1984) posesses all the ingredients needed to model reactor type structures; so we coded their formulation into the NEPTUNE code. The element is based upon Mindlin plate theory and uses a velocity strain formulation that permits large strains.

The above element was primarily developed for metallic structures. For the purpose of modelling RC structures, the above element was enhanced with a model to represent arbitrarily positioned reinforcing bars, a liner model to represent a liner's membrane response, and a material model for concrete, which is described in the next section.

It will be helpful to our subsequent development to first present some key results obtained by Belytschko et al. (1984) for the element. The velocity strain, $\hat{d}_{ij}$, is given by

$$\hat{d}_{xx} = B_{1I}\,\hat{v}_{xI} + \hat{z}\,B_{1I}\,\hat{\theta}_{yI}$$

$$\hat{d}_{yy} = B_{2I}\,\hat{v}_{yI} - \hat{z}\,B_{2I}\,\hat{\theta}_{xI} \qquad (1)$$

$$2\,\hat{d}_{xy} = B_{2I}\,\hat{v}_{xI} + B_{1I}\,\hat{v}_{yI} + \hat{z}\,(B_{2I}\,\hat{\theta}_{yI} - B_{1I}\,\hat{\theta}_{xI})$$

where $\hat{v}_{iI}$ and $\hat{\theta}_{iI}$ are the velocity and angular velocity at node I in the ith local coordinate direction and $\hat{z}$ is the depth coordinate. The forms for B_{iI} are given by

$$B_{iI} = \frac{1}{2\hat{A}} \begin{cases} \begin{bmatrix} \hat{y}_{24} & \hat{y}_{31} & \hat{y}_{42} & \hat{y}_{13} \end{bmatrix}, & \text{(for } i = 1\text{)} \\ \begin{bmatrix} \hat{x}_{42} & \hat{x}_{13} & \hat{x}_{24} & \hat{x}_{31} \end{bmatrix}, & \text{(for } i = 2\text{)} \end{cases} \qquad (2)$$

where $\hat{x}_I$ is the local x coordinate and $\hat{x}_{IJ}$ is the difference between nodal coordinates (e.g. $\hat{x}_{42} = \hat{x}_4 - \hat{x}_2$).

The nodal internal forces are given by

$$\hat{f}_{xI} = A(B_{1I}\,\hat{f}_x + B_{2I}\,\hat{f}_{xy})$$

$$\hat{f}_{yI} = A(B_{2I}\,\hat{f}_y + B_{1I}\,\hat{f}_{xy})$$

$$\hat{f}_{zI} = A\bar{\kappa}(B_{1I}\,\hat{f}_{xz} + B_{2I}\,\hat{f}_{xy}) \qquad (3)$$

$$\hat{m}_{xI} = A[B_{2I}\,\hat{m}_y + B_{1I}\,\hat{m}_{xy} - 0.25\,\bar{\kappa}\,\hat{f}_{yz}]$$

$$\hat{m}_{yI} = A[-B_{1I}\,\hat{m}_x - B_{2I}\,\hat{m}_{xy} + 0.25\,\bar{\kappa}\,\hat{f}_{xz}]$$

$$\hat{m}_{zI} = 0$$

where $\bar{\kappa}$ is the shear factor, and A is the planar area of the element. The element's internal forces, $\hat{f}_{\alpha\beta}$, and internal moments, $\hat{m}_{\alpha\beta}$, are obtained from

$$\hat{f}_{\alpha\beta} = \int \hat{\sigma}_{\alpha\beta}\,d\hat{z}\,, \qquad \hat{m}_{\alpha\beta} = -\int \hat{z}\,\hat{\sigma}_{\alpha\beta}\,d\hat{z}\,, \qquad (4)$$

in which $\hat{\sigma}_{\alpha\beta}$ are corotational stresses.

The element's internal forces and moments due to the response of concrete, $\hat{f}^{con}_{\alpha\beta}$ and $\hat{m}^{con}_{\alpha\beta}$, are computed from eq. (4) in which the concrete stresses, $\hat{\sigma}^{con}_{\alpha\beta}$, are obtained from the concrete material model, which is described below; thus

$$\hat{f}^{con}_{\alpha\beta} = \int \hat{\sigma}^{con}_{\alpha\beta}\,d\hat{z}, \qquad \hat{m}^{con}_{\alpha\beta} = -\int \hat{z}\,\hat{\sigma}^{con}_{\alpha\beta}\,d\hat{z}\,. \qquad (5)$$

Reinforcing Bar Model

The first enhancement to the element is a model for the reinforcing bars. The rebars are represented in the element by discrete layers of smeared reinforcing steel (Fig. 2). Within the element, individual layers are used to represent corresponding layers of actual reinforcement. The following geometric information is required for each layer of rebars: the distance, z (Fig. 3), from the centroidal plane, the angle, θ, that the bars make relative to side 1 of the element, the bar's true cross-sectional area, A_b, and the spacing (pitch) between bars, p. The strain along the bar direction is obtained from the following procedure. The velocity strain, $\hat{d}^{\ell}_{ij}$, in terms of the elements corotational coordinate system at a rebar level, $\bar{z}^{\ell}$, is given by

$$\hat{d}^{\ell}_{xx} = B_{1I}\,\hat{v}_{xI} + \hat{z}^{\ell}\,B_{1I}\,\hat{\theta}_{yI}$$

$$\hat{d}^{\ell}_{yy} = B_{2I}\,\hat{v}_{yI} - \hat{z}^{\ell}\,B_{2I}\,\hat{\theta}_{xI} \qquad (6)$$

$$2\,\hat{d}^{\ell}_{xy} = B_{2I}\,\hat{v}_{xI} + B_{1I}\,\hat{v}_{yI} + \hat{z}^{\ell}\,(B_{2I}\,\hat{\theta}_{yI} - B_{1I}\,\hat{\theta}_{xI})\,.$$

At this point it should be noted that the quantities B_{iI}, v_{iI}, and $\hat{\theta}_{iI}$ do not have to be computed for the rebar response because they were previously computed for the response of the concrete plate. The velocity strain along the bar direction is given by

$$\hat{d}^{\ell}_b = \hat{d}^{\ell}_{xx}\cos^2\theta + \hat{d}^{\ell}_{yy}\sin^2\theta + 2\,\hat{d}^{\ell}_{xy}\sin\theta\cos\theta\,. \qquad (7)$$

The stress, $\bar{\sigma}^{\ell}_b$, in the bars in layer ℓ is assumed to be uniaxial and to lie along the length of the bar. A uniaxial elastoplastic constitutive relationship is used to compute the stress from the strain along the bar direction. The discrete-bar stress, $\bar{\sigma}^{\ell}_b$, is converted into an equivalent smeared reinforcing layer stress, $\bar{\sigma}^{\ell}_s$, according to

$$\bar{\sigma}^{\ell}_s = \frac{\sqrt{\bar{A}}}{p^{\ell}}\,\bar{\sigma}^{\ell}_b\,. \qquad (8)$$

The layer stress is then transformed into a stress state $(\hat{\sigma}^{\ell}_{xx}, \hat{\sigma}^{\ell}_{yy}, \hat{\sigma}^{\ell}_{xy})$ in the local element coordinate system $(\hat{x},\hat{y})$ according to

$$\hat{\sigma}^{\ell}_{xx} = \bar{\sigma}^{\ell}_s\cos^2\theta$$

$$\hat{\sigma}^{\ell}_{yy} = \bar{\sigma}^{\ell}_s\sin^2\theta \qquad (9)$$

$$\hat{\sigma}^{\ell}_{xy} = 2\,\bar{\sigma}^{\ell}_s\sin\theta\cos\theta$$

The internal forces, $\hat{f}^{rb}_{\alpha\beta}$, and internal moments, $\hat{m}^{rb}_{\alpha\beta}$, in Eq. (4) due to the smeared layers of rebars are computed from

$$\hat{f}^{rb}_{\alpha\beta} = \sum_{\ell=1}^{L} \frac{A^{\ell}}{p^{\ell}} \hat{\sigma}^{\ell}_{\alpha\beta}$$

and (10)

$$\hat{m}^{rb}_{\alpha\beta} = - \sum_{\ell=1}^{L} \hat{z}^{\ell} \frac{A^{\ell}}{p^{\ell}} \hat{\sigma}^{\ell}_{\alpha\beta}$$

where ℓ is a rebar layer number and L is the number of rebar layers.

Liner Model

The second enhancement to the quadrilateral plate element was a model that accounts for the membrane response of the liner. The liner is located on an outside surface of the element at $\hat{z}^{lr}$. The velocity strains in the liner are obtained from Eq. (1) when z is replaced by $\hat{z}^{lr}$. The velocity strains are then used in our existing constitutive subroutine for metals to obtain the current corotational membrane stress in the liner, $\hat{\sigma}^{lr}_{\alpha\beta}$. The element's internal forces due to the membrane response of the liner are given by

$$\hat{f}^{lr}_{\alpha\beta} = \hat{\sigma}^{lr}_{\alpha\beta} h , \qquad \hat{m}^{lr}_{\alpha\beta} = - \hat{z}^{lr} \hat{\sigma}^{lr}_{\alpha\beta} h , \qquad (11)$$

where h is the thickness of the liner.

The element's internal forces and moments are equal to the sum of the contributions from the responses of the concrete, rebars, and liner, that is

$$\hat{f}_{\alpha\beta} = \hat{f}^{con}_{\alpha\beta} + \hat{f}^{rb}_{\alpha\beta} + \hat{f}^{lr}_{\alpha\beta} ,$$

(12)

$$\hat{m}_{\alpha\beta} = \hat{m}^{con}_{\alpha\beta} + \hat{m}^{rb}_{\alpha\beta} + \hat{m}^{lr}_{\alpha\beta} .$$

The results of Eq. (12) are used in Eq. (3) to obtain the nodal internal forces for a lined, reinforced concrete plate element.

Now we would like to emphasize the fact that by incorporating the rebar and membrane liner computations into the subroutine that computes the response of the concrete shell, a large reduction in computational effort is achieved over that needed if separate elements would have been used for the concrete shell, rebar, and liner.

MATERIAL RESPONSE MODELS

This section describes the material response models used for concrete, for the liner plate, and for the reinforcing bars.

The material model for concrete implemented into NEPTUNE was the model (Takahashi, 1983 and Pfeiffer, 1986) originally developed for the TEMP-STRESS code (Marchertas et al., 1988). The model accounts for the significant difference in tensile and compressive behavior as indicated by a typical uniaxial compression-tension stress-strain curve shown in Fig. 4. The strain hardening part of the behavior is modelled with a von Mises loading function (Fig. 5) and failure is detected with the Hsieh-Ting-Chen four-parameter model (Hsieh et al., 1982). The post-failure response of concrete in the tension regime (tension softening) follows the element-size-independent cracking criterion of Bazant and Oh (1983). The energy release rate is used as a strain-softening parameter to control the cracking behavior. To account for the orthotropic softening in the element after cracking, an orthotropic stiffness matrix (Pfeiffer, 1986) is employed. Compression softening is modelled through the von Mises loading function in which an isotropic stiffness matrix is used.

The liner plate is usually constructed from steel. A two-dimensional elastoplastic strain hardening material model with the von Mises yield criterion is used to represent the liner steel. Failure of the liner is assumed to occur when the calculated equivalent true-strain exceeds the value for the ultimate strain.

The reinforcing bars are assumed to be in a uniaxial state of stress. Therefore, a uniaxial elastoplastic strain hardening material model is used to represent the material response. A multilinear true stress-true strain curve, obtained from experimental data when available, is used in the constitutive algorithm. Rebar failure is assumed to occur in tension when the calculated axial strain exceeds the value of the ultimate strain.

An important failure mode that can occur in reinforced concrete structures is transverse shear failure. The transverse shear force acts perpendicular to the surface of the plate, and it is usually largest at wall-base junctions and at corners. A comprehensive treatment of this failure mode would have to include the interaction among concrete cracking, friction and aggregate interlock, and the dowel action of the rebars.

The element described above cannot be used to obtain the transverse shear failure mode based upon a comprehensive treatment of the mechanics for the following reasons. The plate element that is being used to represent reinforced concrete sections is a Mindlin type of element. The transverse shear stresses $\hat{\sigma}_{\alpha\beta}$ are computed from the shear strains, $\hat{\gamma}_{\alpha\beta}$ by

$$\hat{\sigma}_{\alpha\beta} = G \hat{\gamma}_{\alpha\beta} \qquad (13)$$

where G is the elastic shear modulus, as opposed to being coupled to the other stresses through a constitutive relation. Also, the transverse shear stress distribution through the thickness is assumed constant. The reason for this is that the transverse shear term acts as a penalty term to enforce the Kirchhoff condition. In addition, the shear stress is ignored in the modelling of the rebars and there is no interaction between the rebars and concrete.

From the above it is seen that detailed modelling of the transverse shear failure mode is not feasible with the simplified models for the rebars, concrete, and their interaction that are currently being used in the code. Therefore, an empirical approach was employed to evaluate the ultimate transverse shear

strength. The method adopted is based upon an empirical formula developed by Aoyagi and Yamada (1979) who conducted experiments on reinforced concrete flat plate specimens subjected to combined shear and axial loads. They found that the lower bound for the ultimate shear strength, τ^u, is the smaller value computed from

$$\tau^u = [\beta_1(\rho\sigma^y - \sigma_{nn}) + \beta_2] \ (f'_c)^{0.5}$$
$$\tau^u = \beta_3 \ (f'_c)^{0.5} \qquad (14)$$

where β_1, β_2 and β_3 are constants, which depend upon the dimensional units being used, ρ is the reinforcement ratio in the normal direction, which is the area of steel divided by gross cross section area of the element A_g, σ^y is the yield stress of the reinforcing steel, σ_{nn} is the average normal stress, and f'_c is the ultimate shear strength of concrete. The constants β_1, β_2 and β_3 are given in Table 1 for several sets of dimensional units. The average transverse shear stress, σ_{nz}, and the average normal stress, σ_{nn}, in the element are computed from

$$\hat{\sigma}_{nz} = \frac{\hat{f}_{nz}}{A_g} \ , \ \hat{\sigma}_{nn} = \frac{\hat{f}_{nn}}{A_g} \qquad (15)$$

The average normal stress is used in Eq. (14) to evaluate the ultimate shear strength. The computed average shear stress of Eq. (15) is then compared to the ultimate shear stress of Eq. (14) to determine if a transverse shear failure occurred.

SOLUTION ALGORITHM

The equations that are to be solved for a static analysis are the equilibrium equations given by

$$f_{iI}^{int} = f_{iI}^{ext} \ , \qquad (16)$$

where f_{iI}^{int} and f_{iI}^{ext} are the internal and external nodal forces, respectively, of node I in the ith direction. For dynamic problems, the governing equations are the semidiscretized equations of motion which are given by

$$m_{iI} \ddot{u}_{iI} + f_{iI}^{int} = f_{iI}^{ext} \ , \quad \text{(no sum)} \qquad (17)$$

where m_{iI} is a diagonal mass matrix and u_{iI} is a nodal displacement. Superscript dots are used to denote temporal derivatives. Here we note that NEPTUNE was originally developed as a dynamic code; static analysis capability is a very recent addition. The equations of motion are solved using the central difference formulas.

From the various methods that are available for obtaining static solutions, we selected the method of dynamic relaxation (DR), which was apparently introduced by Otter (1965). A recent summary of the method is given by Underwood (1983). The three main reasons for this choice of method were: (1) it is applicable to highly nonlinear problems, which occur in structural safety evaluations, (2) it requires minimal changes to the NEPTUNE code's architecture, and (3) it does not require additional storage beyond that required by the central difference method. The equations that are to be solved for a static analysis are the static equilibrium equations given by Eq. (16). With the DR method, the solution of Eq. (16) is obtained as the damped solution to the equations of motion (i.e. Eq. (17)) in which the mass matrix is chosen to minimize the number of steps for convergence. Thus, in effect we are essentially solving the same equations for both the dynamic and static cases. Of course there are some minor differences in the solution procedure which we will now highlight.

The updates for the acceleration, velocity, and displacement are given by

$$\ddot{u}_{iI}^{n} = m_{iI}^{-1} \ (f_{iI}^{ext,n} - f_{iI}^{int,n}) \ , \quad \text{(no sum)} \qquad (18)$$

$$\dot{u}_{iI}^{n+1/2} = \alpha_1 \ \dot{u}_{iI}^{n-1/2} + \alpha_2 \ \Delta t \ \ddot{u}_{iI}^{n} \ , \qquad (19)$$

$$u_{iI}^{n+1} = u_{iI}^{n} + \Delta t \ \dot{u}_{iI}^{n+1/2} \ , \qquad (20)$$

where Δt is the time increment and n is the step number ($n = 0, N_{max}$; N_{max} = maximum number of steps). Note, a special starting procedure is used since the value for $\dot{u}_{iI}^{n-1/2}$ when n=0 is not known. For n=0, Eq. (19) is replaced by

$$\dot{u}_{iI}^{1/2} = \frac{\Delta t}{2} \ \ddot{u}_{iI}^{0} \ . \qquad (21)$$

The parameters α_1 and α_2 in Eq. (19) take on different values for static and dynamic analysis. For the dynamic case, both α_1 and α_2 are equal to one ($\alpha_1 = \alpha_2 = 1.0$) and the updates in Eqs. (19) and (20) are reduced to the standard central difference updates. For the static case, α_1 and α_2 are given by

$$\alpha_1 = \frac{2 - c \ \Delta t}{2 + c \ \Delta t} \ , \ \alpha_2 = \frac{2}{2 + c \ \Delta t} \qquad (22)$$

where c is the damping. The damping value is determined from

$$c = 2 \ \omega_\ell \qquad (23)$$

where ω_ℓ is the lowest participating frequency of the system. The lowest frequency is determined each step using an approximate Rayleigh quotient (e.g. Underwood, 1983) according to

$$\omega_\ell^2 = \frac{u_{iI} \ u_{iI} \ K_{iI}}{u_{iI} \ u_{iI} \ m_{iI}} \ , \ \text{(sum over i, I)} \qquad (24)$$

where K_{iI} is a diagonal approximate stiffness matrix whose terms are computed at each step by

$$K_{iI}^{n} = [f_{iI}^{int,n} - f_{iI}^{int,n-1}]/[\Delta t \ \dot{u}_{iI}^{n-1/2}] \ . \qquad (25)$$

Note, if K_{iI}^{n} is less than zero, it is set equal to zero.

In order to reduce the number of steps required for convergence, the element densities are chosen such

that the element transit times are all identical. In our work we have chosen $\Delta t = 1$. Convergence is assumed when the following criteria are satisfied.

$$\frac{\left\| f_{iI}^{ext,n} - f_{iI}^{int,n} \right\|_2}{\left\| f_{iI}^{ext,n} \right\|_2} \times 100 \leq \epsilon_f \qquad (26)$$

$$\frac{\left\| \dot{u}_{iI}^{n+1/2} \Delta t \right\|_2}{\left\| u_{iI}^{n+1} \right\|_2} \times 100 \leq \epsilon_u \qquad (27)$$

where $\| \quad \|_2$ indicates the Euclidean norm. We have found that $\epsilon_f = 0.1$ and $\epsilon_u = 0.001$ usually produce accurate results without excessive computations.

VISUALIZATION

The safety analysis of reactor structures oftentimes leads to the use of large complex finite element models that must be plotted to verify their correctness. In addition to the normal display requirements of finite element meshes, reinforced concrete structures require two additional plotting features: the display of the topology of the reinforcing bars and the display of the computed cracking pattern.

The above features have been incorporated into our preprocessor code, PRENEP and postprocessor code, POSTNEP (Kulak and Fiala, 1988). Typical reinforced concrete sections contain multiple layers of reinforcing steel. The following scheme was developed to display the orientation of the rebars. The finite elements of the mesh are indicated by dotted lines and the rebars by a solid line passing through the center of each element. For the purpose of maintaining clarity, only one rebar per direction per element is drawn through the center of the element, and a maximum of two rebar layers can be displayed. The orientation of the rebars is shown relative to the global axis, which corresponds to its location in the physical world. Illustrated in Fig. 6 is a representative display of an element containing orthogonal reinforcement.

In order to graphically capture the degradation of RC structures, the capability to display cracking and crushing of concrete has been added. Figure 7 shows that a crack is represented by a dashed line within the element, and crushing is represented by dots within the element. Note, multiple cracks are illustrated in some of the elements.

Additional illustrations of the above display features are provided in the sample problem. These feature provide the analyst with significant visual aid to understand the response of complex RC structures.

CONCRETE CONTAINMENT RESPONSE TO STATIC OVERPRESSURE

Here we describe pretest numerical simulations of the response of a 1/6th-scale reinforced concrete containment model, designed and constructed for the U. S. Nuclear Regulatory Commission, and tested to failure by static overpressurization. The test was conducted at Sandia National Laboratories during the middle of 1987. One of the purposes of the test was to validate current analytical and numerical methods for predicting response up to failure.

Description of Containment Experimental Model

The 1/6th scale concrete containment model is depicted in Fig. 8. A steel liner provides a leak tight boundary. Headed studs attached to the liner are used to affix the liner to the concrete along the cylinder and dome. A thick reinforced foundation mat is the bottom pressure boundary. Several penetrations, such as equipment hatches, personnel airlock representations, and smaller pipes, are located in the cylinder. The wall sections around the equipment hatches are thickened.

A considerable amount of reinforcing steel was placed in the cylinder, dome, basemat, and around the penetrations. Specifications for the placement of the rebars is given by Clauss (1987).

Material Properties

Both the liner and rebars were modelled as isotropic hardening elastoplastic materials. The liner properties are taken to be as follows: Young's modulus = 30×10^6 psi (207 GPa), Poisson's ratio = 0.3, yield stress = 50.2×10^3 psi (346 MPa), ultimate strength = 70×10^3 psi (483 MPa) at a strain of 16.4%. The rebar properties are given by: Young's modulus = 31×10^6 psi (214 GPa), Poisson's ratio = 0.3, yield stress = 66.6×10^3 psi (459 MPa), ultimate strength = 99×10^3 psi (683 MPa) at a strain of 4.6%.

The Hsieh-Ting-Chen four parameter failure surface is used to characterize the strength of concrete. The properties of concrete are given by: Young's modulus = 4.8×10^6 psi (33.1 GPa), Poisson's ratio = 0.2, compressive strength = 6.8×10^3 psi (46.9 MPa), and tensile strength = 500 psi (3.5 MPa).

Finite Element Model

The 1/6th scale concrete containment model (Fig. 8) contains several large penetrations, such as an equipment hatch and personnel lock, that will cause deviations from a pure axisymmetric response and may decrease the capacity of the containment. In order to predict the behavior near these regions, a nominal 50 degree circumferential segment of the model was developed (Fig. 9). The segment includes the cylinder from the basemat to the springline and the dome. The cylinder portion contains one-half of the penetration opening for Equipment Hatch "B". The basemat was not included in this model; thus, its effects on the cylinder at the cylinder-basemat junction are not taken into account.

The topology of the reinforcement was specified for each element by prescribing the location of each layer in the depth direction and the orientation relative to side 1 of the element. The circumferential, meridional, and seismic rebar topology is captured fairly accurately in regions remote from the penetration. The curved shape of the rebars near the penetration is approximated by straight bars within each element, but the orientation of the bars from small groups of contiguous elements to adjacent small groups of contiguous elements is varied to globally capture the curved shape. Figure 10 shows the layout of the rebars in layer 4 and 5 within the cylinder and dome.

The model is subjected to a fixed boundary condition (no translations or rotations allowed) at the base of the cylinder. Symmetry conditions are enforced on the nodes that lie in each of the two vertical symmetry

planes; the first plane contains the meridional edge of the model with the penetration opening, and the second plane contains the other meridional edge. The symmetry boundary condition is a roller condition in which motion (translational and rotational) is only allowed in the symmetry plane. The apex node is only permitted to move in the vertical direction; no rotations are allowed.

The load is a pressure incrementally applied to the inside surface of the containment and a line load, which is equivalent to the pressure load on the hatch cover, applied in the radial direction to the edge of the penetration opening in the updated geometry. A pressure of 20 psig is applied in the first load step, and 5 psig increments are used thereafter.

Results

The model was pressurized incrementally up to failure, which occurred at 185 psig (1.276 MPa). All materials in the model behaved elastically up to 25 psig (0.172 MPa). Cracking at the inner diameter of the boss at the 6 and 12 o'clock positions began at the pressure of 30 psig (0.207 MPa). Meridional cracks also formed at the base of the cylinder. The predicted cracking pattern on the inside surface of the containment at 40 psig is visible in Fig. 11. It was noted that the radial displacements of the cylinder near the region of the boss and including the boss were less than those further away. This deformation pattern formed an inward dimple as shown in Fig. 12, in which the displacements have been magnified by a factor of 5. Beginning at 40 psig (0.276 MPa), extensive cracking occurred in the boss, cylinder, and dome. The liner material begins to behave plastically at 85 psig (0.586 MPa). Stress in the hoop reinforcement reached the yield value at 125 psig (0.862 MPa), and the meridional rebars were stressed to yield at 145 psig (1.000 MPa). A splice in a layer 6 (hoop) rebar failed at point A shown in Fig. 12 during the load increment from 180 psig (1.241 MPa) to 185 psig (1.276 MPa). The radial and vertical displacements at the vessel springline are shown in Fig. 13. Figure 14 shows the variation in diameter with pressure of the equipment hatch in the horizontal and vertical directions. This ovalization could create a potential leakage path if the seal between the hatch and cover is distorted enough. A more complete report of this simulation is given by Clauss (1987).

ACKNOWLEDGEMENTS

This work was performed under the auspices of the U.S. Department of Energy, Office of Technology Support Programs, under contract W-31-109-Eng-38.

REFERENCES

Aoyagi, Y. and Yamada, K., 1979, "An Experimental Approach to the Design of Network Reinforcement Against In-Plane Shear in Reinforced Concrete Containments," Transactions, 5th International Conference on Structural Mechanics in Reactor Technology, A. Jaeger and B. A. Boley, ed., North-Holland Publishing Co., Amsterdam, Vol. J, paper J 4/7.

Bazant, Z. P. and Oh, B. H., 1983, "Crack Band Theory for Fracture of Concrete," Materiaux et Constructions, Vol. 16, pp. 155-177.

Belytschko, T., Lin, J. I., and Tsay, C-S., 1984, "Explicit Algorithms for Nonlinear Dynamics of Shells," Computer Methods in Applied Mechanics and Engineering, Vol. 42, pp. 225-251.

Clauss, D. B., ed., 1987, "Round-Robin Pretest Analysis of a 1:6-Scale Reinforced Concrete Containment Model Subject ot Static Internal Pressurization," Sandia National Laboratory Report, NUREG/CR-4913, SAND87-0891.

Hsieh, S.S., Ting, E. C., and Chen, W. F., 1982, "A Plastic-fracture Model for Concrete," International Journal of Solids and Structures, Vol. 18, No. 3, pp. 181-197.

Kulak, R. F., and Fiala, C., 1988, "NEPTUNE: A System of Finite Element Programs for Three-Dimensional Nonlinear Analysis," Nuclear Engineering and Design, Vol. 106, pp. 47-68.

Marchateras, A. H., Kennedy, J. M., and Pfeiffer, P.A., 1988, "Reinforced Flexural Elements for TEMP-STRESS Programs," Nuclear Engineering and Design, Vol. 106, pp. 87-102.

Otter, J. R. H., 1965, "Computations for Prestressed Concrete Reactor Pressure Vessels Using Dynamics Relaxation," Nuclear Structural Engineering, Vol. 1, pp. 61-75.

Pfeiffer, P. A., 1986, "Size Effect in Blunt Fracture," Ph.D. Thesis, Northwestern University, Evanston, IL USA.

Takahashi, Y., 1983, "Elastic-plastic Constitutive Modelling of Concrete," Argonne National Laboratory Report, ANL-83-23.

Underwood, P., 1983, "Dyanmic Relaxiation," in: Computational Methods for Transient Analysis, T. Belytschko and T. J. R. Hughes, ed., North Holland Publishing Co., Amsterdam, pp. 245-266.

Table 1. Constant for Ultimate Transverse Shear Strength Criteria

Units	β_1	β_2	β_3
MPa	0.160	0.157	1.41
lb/in^2	0.013	1.9	17.0
kgf/cm^2	0.05	0.5	4.5

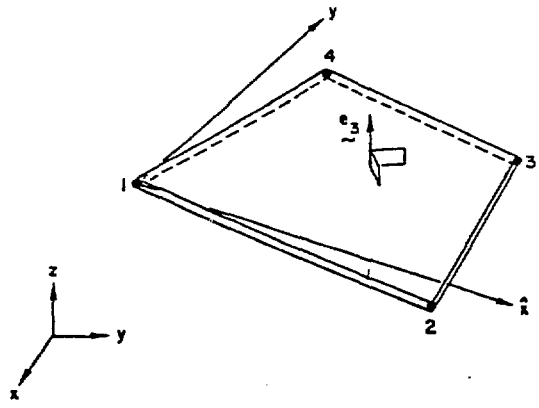

Fig. 1. Basic Quadrilateral Plate Element.

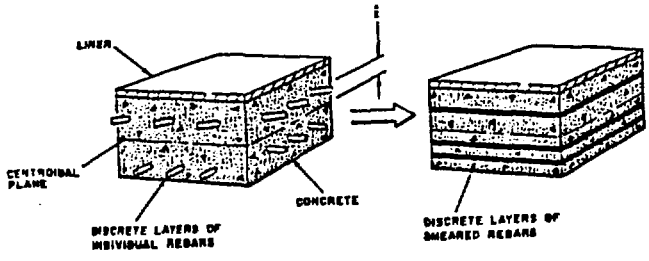

Fig. 2. Representation of Layers of Individual Rebars as Layers of Smeared Rebars.

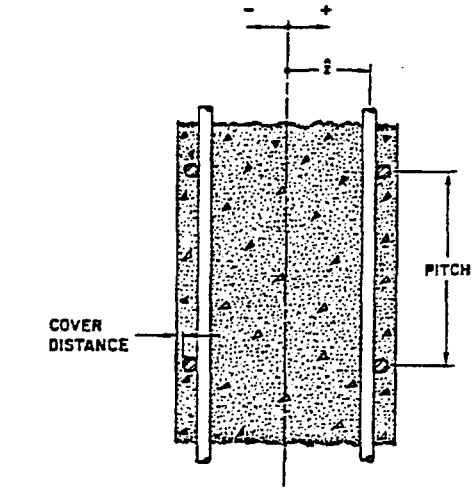

Fig. 3. Position of Rebar within Concrete Slab/Wall.

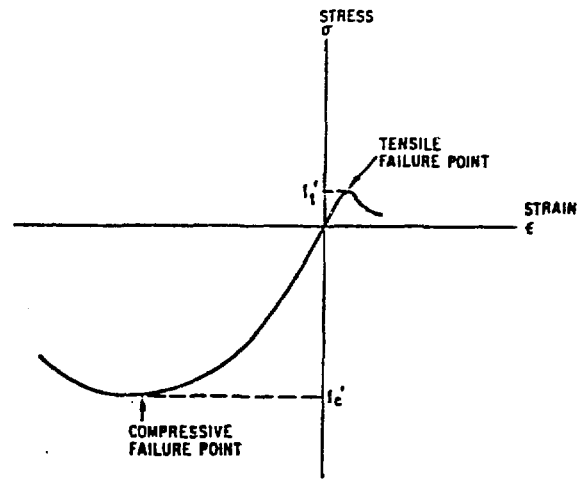

Fig. 4. Uniaxial Response of Concrete in Tension and Compression.

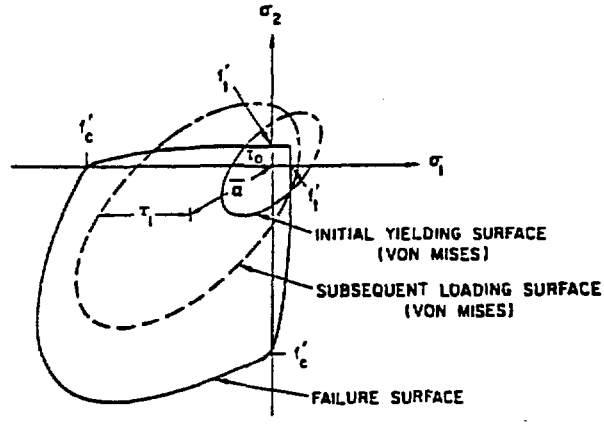

Fig. 5. Loading and Failure Surfaces.

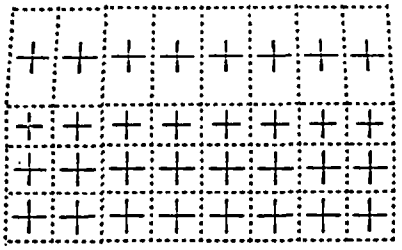

Fig. 6. Display of Reinforcing Bars.

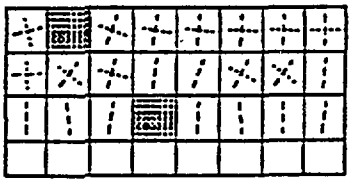

Fig. 7. Display of Concrete Cracking and Crushing.

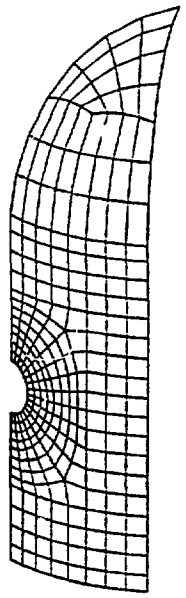

Fig. 9. Finite Element Model of 1/6th Scale Concrete Containment Test.

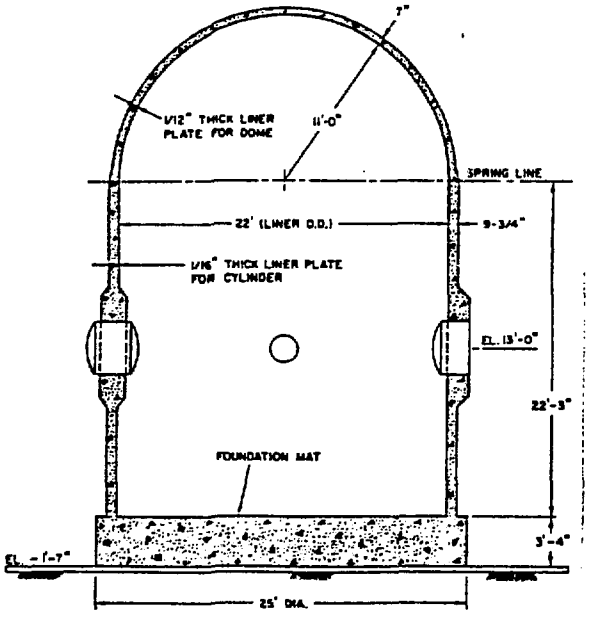

Fig. 8. Schematic of 1/6th Scale Concrete Containment Model.

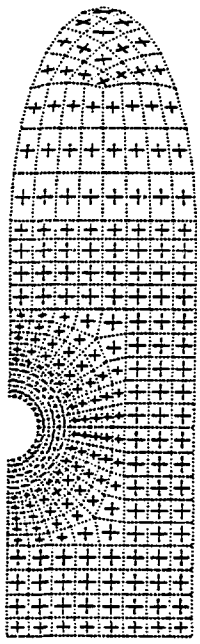

Fig. 10. Layout of Rebars for Layer 4 and 5.

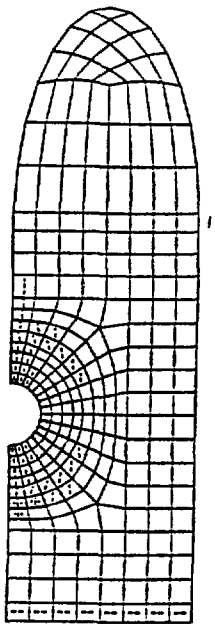

Fig. 11. Cracking Pattern on Inside Surface at 40 psig.

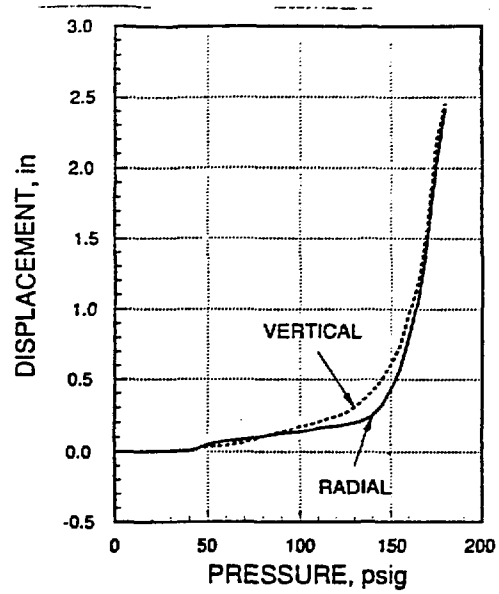

Fig. 13. Radial and Vertical Displacement at Vessel Springline.

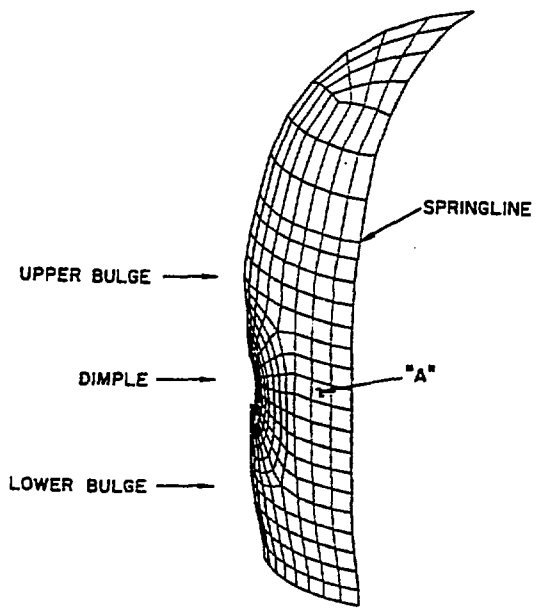

Fig. 12. Predicted Deformed Configuration of Finite Element Containment Model.

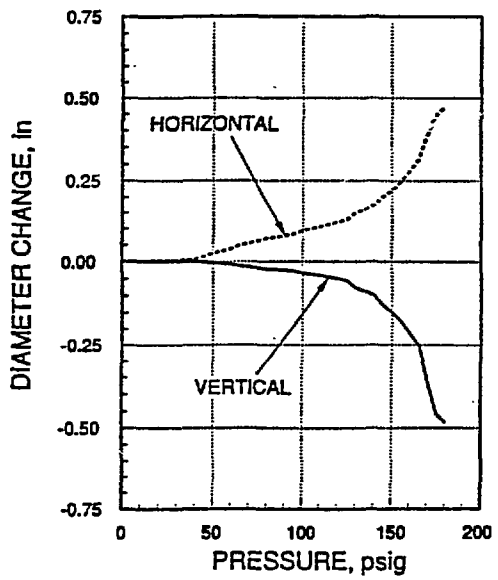

Fig. 14. Change in Horizontal and Vertial Diameters of Equipment Hatch.